ADVANCES IN ATMOSPHERIC SCIENCES, VOL. 33, OCTOBER 2016, 1137–1142

Precipitation Responses to Radiative Effects of Ice Clouds: A Cloud-Resolving Modeling Study of a Pre-Summer Torrential Precipitation Event

Xinyong SHEN*[1], Wenyan HUANG[2], Chunyan GUO[3], and Xiaocen JIANG[1]

[1]*Key Laboratory of Meteorological Disaster, Ministry of Education/Joint International Research Laboratory of Climate and Environment Change/Collaborative Innovation Center on Forecast and Evaluation of Meteorological Disasters, Nanjing University of Information Science and Technology, Nanjing, Jiangsu* 210044*, China*

[2]*Changzhou Meteorological Bureau, Changzhou, Jiangsu* 213022*, China*

[3]*Inner Mongolia Meteorological Service Center, Hohhot, Inner Mongolia* 010051*, China*

(Received 20 October 2015; revised 9 February 2016; accepted 24 February 2016)

ABSTRACT

The precipitation responses to the radiative effects of ice clouds are investigated through analysis of five-day and horizontally averaged data from 2D cumulus ensemble model experiments of a pre-summer torrential precipitation event. The exclusion of the radiative effects of ice clouds lowered the precipitation rate through a substantial reduction in the decrease of hydrometeors when the radiative effects of water clouds were switched on, whereas it increased the precipitation rate through hydrometeor change from an increase to a decrease when the radiative effects of ice clouds were turned off. The weakened hydrometeor decrease was associated with the enhanced longwave radiative cooling mainly through the decreases in the melting of non-precipitating ice to non-precipitating water. The hydrometeor change from an increase to a decrease corresponded to the strengthened longwave radiative cooling in the upper troposphere through the weakened collection of non-precipitating water by precipitation water.

Key words: hydrometeor change, precipitation rate, longwave radiative cooling, local atmospheric cooling

Citation: Shen, X. Y., W. Y. Huang, C. Y. Guo, and X. C. Jiang, 2016: Precipitation responses to radiative effects of ice clouds: A cloud-resolving modeling study of a pre-summer torrential precipitation event. *Adv. Atmos. Sci.*, **33**(10), 1137–1142, doi: 10.1007/s00376-016-5218-8.

1. Introduction

Solar shortwave radiative heating and infrared longwave radiative cooling are crucial to the thermal balance and vertical stratification during the development of precipitation systems. The radiative difference between cloudy and cloud-free areas leads to a nocturnal precipitation peak through the enhancement of secondary circulation (Gray and Jacobson, 1977). Cloud radiative processes affect the unstable vertical temperature structure associated with upper-tropospheric stratiform clouds (Lilly, 1988) and the destabilization of the environment (Dudhia, 1989). Tao et al. (1993) conducted cloud-resolving model experiments and found that the longwave radiative cooling enhanced precipitation in both the tropics and midlatitudes. Sui et al. (1997, 1998), Gao et al. (2009) and Gao and Li (2010) showed that the nocturnal temperature decrease induced by the infrared radiative cooling lowers the saturation mixing ratio and increases condensation, which produces the nocturnal precipitation peak.

Recently, Shen et al. (2011b) showed that the exclusion of radiation enhances the daily and horizontally averaged precipitation rate during the onset and dissipation phases, but it weakens the average precipitation rate during the peak phase. Wang et al. (2010b) found that the removal of the radiative effects of ice clouds lowers the average precipitation rate during the onset and development phases, whereas it increases the average precipitation rate during the peak and dissipation phases. Shen et al. (2011a) revealed that the elimination of the radiative effects of water clouds lowers the average precipitation rate during the peak phase but increases it during the dissipation phase. Liu et al. (2014) further studied the responses of five-day and horizontally averaged heat, cloud microphysical and surface precipitation budgets to the radiative effects of water clouds. When the radiative effects of ice clouds were switched on, the exclusion of the radiative effects of water clouds lowered the horizontally averaged precipitation rate through decreases in the melting of ice crystals caused by enhanced local atmospheric cooling. When the radiative effects of ice clouds were switched off, the removal of the radiative effects of water clouds increased the average precipitation rate through the strengthened net condensation

* Corresponding author: Xinyong SHEN
Email: shenxy@nuist.edu.cn

and the reduction in the melting of ice crystals related to enhanced lower-tropospheric longwave radiative cooling.

Wang et al. (2010b) studied the precipitation responses to the radiative effects of ice clouds only when the radiative effects of water clouds were turned on. But what would the precipitation responses be to the radiative effects of ice clouds when the radiative effects of water clouds are switched on and off, respectively? How do the radiative effects of ice clouds affect cloud microphysics and the precipitation rate? The objective of this study is to examine the cloud microphysical and thermal responses to the radiative effects of ice clouds, and this is approached by analyzing model-simulated data averaged over five days and the model domain. The difference in the average precipitation rate caused by the exclusion of the radiative effects of ice clouds is explained by the difference in the vertical profiles of the averaged heat through analysis of the difference in the averaged cloud microphysical budget. The model and experiments are briefly described in section 2. The results are presented in section 3, and summarized in section 4.

2. Model and experiments

Before convection started in this torrential rainfall event, the western Pacific subtropical high extended westward and southwesterly winds were intensified. Warm and humid air transported by the southwesterly winds converged with cold air from the north over southern China. A trough moved into southern China to trigger squall-line convection, which led to torrential rainfall with a maximum rain amount of 482.2 mm in Yangjiang, Guangdong, on 6 June 2008. The model was integrated from 0200 LST 3 June to 0200 LST 8 June 2008 in the control experiment (P). The control simulation was validated with available observational data, including rain gauge (Wang et al., 2010b) and temperature and specific humidity data from GDAS (Shen et al., 2011b). The control experiment and associated sensitivity experiments have been used to study various physical processes associated with the development of precipitation systems. For example, the precipitation responses to vertical wind shear and cloud radiative processes (Shen et al., 2011b) and ice (Wang et al., 2010b, Shen et al., 2011c) and water (Shen et al., 2011a, 2012; Liu et al., 2014) clouds, and the improvement of the simulated depositional growth of ice crystals (Shen et al., 2014; Li et al., 2016).

The model used in this study is the modified 2D cumulus ensemble model (Soong and Ogura, 1980; Soong and Tao, 1980; Tao and Simpson, 1993; Sui et al., 1994, 1998; Li et al., 1999, 2002). The prognostic equations of specific humidity and five cloud species (cloud water, raindrops, cloud ice, snow and graupel) have their source/sink terms from cloud microphysical schemes (Lin et al., 1983; Rutledge and Hobbs, 1983, 1984; Tao et al., 1989; Krueger et al., 1995). The prognostic equation of potential temperature has its source/sink terms from radiation schemes (Chou et al., 1991, 1998; Chou and Suarez, 1994), and the release of latent heat from cloud microphysical schemes. Details on the model, physical package and parameters can be found in Gao and Li (2008) and Li et al. (2011). A description of the large-scale forcing, including vertical velocity and zonal wind, can be found in Shen et al. (2011b, Fig. 1). Such a model setup has been used to successfully simulate and study the tropical precipitation rate during TOGA COARE (Gao et al., 2004, 2005; Shen et al., 2010; Li et al., 2011, 2013, 2014) and for severe tropical storm Bilis in 2006 (Wang et al., 2009a, b, 2010a).

Three sensitivity experiments (PNWR, PNIR and PNCR) were conducted, identical to P except that water, ice and total (both water and ice) hydrometeor mixing ratios were set to zero when radiation was computed. The difference between PNIR and P (i.e., PNIR−P) is analyzed to study the precipitation responses to the radiative effects of ice clouds when the radiative effects of water clouds are switched on. The difference between PNCR and PNWR (i.e., PNCR−PNWR) is analyzed to study the precipitation responses to the radiative effects of ice clouds when the radiative effects of water clouds are turned off.

3. Results

The exclusion of the radiative effects of ice clouds lowered the five-day and horizontally averaged pre-summer precipitation rate from P to PNIR when the radiative effects of

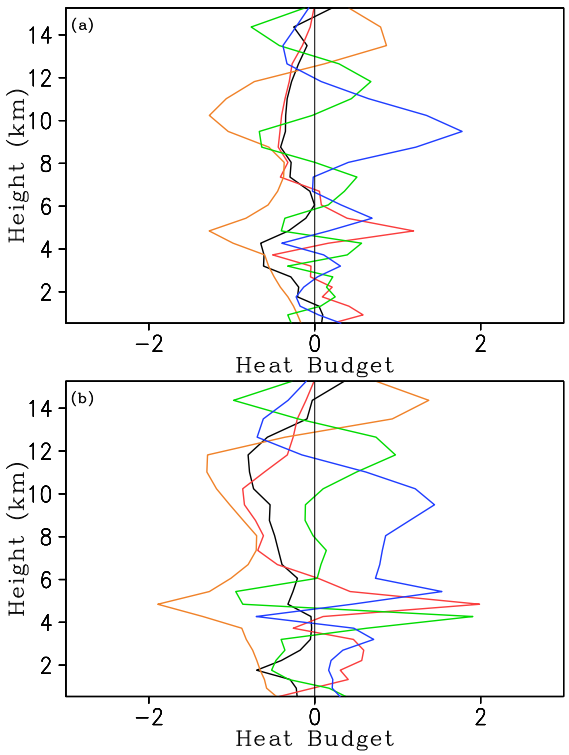

Fig. 1. Vertical profiles of the differences between (a) PNIR and P (PNIR−P) and (b) PNCR and PNWR (PNCR−PNWR) for local temperature change (black), condensational heating (red), convergence of vertical heat flux (green), vertical temperature advection (blue), and radiation (orange), averaged over 5 days and the model domain. Units: °C d^{-1}.

water clouds were switched on, but it increased the average precipitation rate from PNWR to PNCR when the radiative effects of water clouds were turned off (Table 1). To examine the cloud processes responsible for the surface precipitation rate (P_S), the cloud budget is analyzed. The cloud budget is expressed by

$$P_S = Q_{NC} + Q_{CM} , \quad (1)$$

where Q_{NC} is the net condensation and Q_{CM} is hydrometeor change due to cyclic lateral boundaries in the model.

When the radiative effects of water clouds were switched on, the reduction in the average precipitation rate from P to PNIR caused by the exclusion of the radiative effects of ice clouds was associated with the slowdown in the averaged decrease of hydrometeors from P to PNIR (Table 1). When the radiative effects of water clouds were switched off, the increase in the average precipitation rate from PNWR to PNCR resulting from the removal of the radiative effects of ice clouds corresponded to the average hydrometeor change from an increase in PNWR to a decrease in PNCR. The averaged hydrometeor change (Q_{CM}) can be further broken down into the averaged hydrometeor change in cloud water (Q_{CMC}), raindrops (Q_{CMR}), cloud ice (Q_{CMI}), snow (Q_{CMS}) and graupel (Q_{CMG}):

$$Q_{CM} = Q_{CMC} + Q_{CMR} + Q_{CMI} + Q_{CMS} + Q_{CMG} . \quad (2)$$

When the radiative effects of water clouds were switched on, the reduction in the averaged decrease of hydrometeors from P to PNIR caused by the elimination of the radiative effects of ice clouds resulted from the increase in the averaged cloud-water gain, the averaged cloud-ice change from a loss in P to a gain in PNIR, and the reduction in the averaged graupel loss (Fig. 1). The increase in the averaged cloud-water gain from P to PNIR was associated with the slowdown in the collection of cloud water by rain (P_{RACW}) from P to PNIR (Table 2a). The averaged cloud-ice change from a loss in P to a gain in PNIR was related to the decrease in the averaged melting of cloud ice to cloud water (P_{IMLT}) (Table 2b). The reduction in the averaged graupel loss corresponded to the enhancement in the averaged accretion of cloud water by graupel (P_{GACW}) from P to PNIR (Table 2c).

Table 1. Cloud microphysical budgets (P_S, Q_{NC} and Q_{CM}) and the breakdown of Q_{CM} averaged over five days and the model domain in P, PNIR, PNWR, PNCR, and their differences (PNIR−P and PNCR−PNWR). Units: mm d^{-1}.

	P	PNIR	PNWR	PNCR	PNIR−P	PNCR−PNWR
P_S	32.74	31.83	31.73	32.58	−0.91	0.85
Q_{NC}	31.99	31.84	32.33	32.25	−0.15	−0.08
Q_{CM}	0.75	−0.01	−0.60	0.34	−0.76	0.94
Q_{CMC}	−0.03	−0.31	−0.43	−0.25	−0.28	0.18
Q_{CMR}	−0.12	0.24	−0.13	0.57	0.36	0.70
Q_{CMI}	0.50	−0.05	−0.07	−0.13	−0.55	−0.06
Q_{CMS}	−0.10	−0.14	−0.07	0.01	−0.04	0.08
Q_{CMG}	0.50	0.26	0.09	0.14	−0.24	0.05

Table 2. Breakdown of (a) Q_{CMC}, (b) Q_{CMI} and (c) Q_{CMG} in P and PNIR and their differences (PNIR−P). Units: mm d^{-1}. Cloud microphysical processes listed in this table can be found in Table 1.2 in Gao and Li (2008).

(a)	P	PNIR	PNIR−P
Q_{CMC}	−0.03	−0.31	−0.28
P_{SACW}	2.16	2.10	−0.06
P_{RAUT}	0.36	0.40	0.04
P_{RACW}	23.46	22.31	−1.15
$-P_{IMLT}$	−0.84	0.00	0.84
$P_{GACW}(T > T_0)$	10.62	11.09	0.47
$-P_{CND}$	−35.89	−36.31	−0.42
(b)	**P**	**PNIR**	**PNIR−P**
Q_{CMI}	0.50	−0.05	−0.55
P_{SAUT}	4.66	4.42	−0.24
P_{SACI}	0.20	0.29	0.09
P_{SFI}	1.42	1.91	0.49
P_{GACI}	0.26	0.30	0.04
P_{IMLT}	0.84	0.00	−0.84
$-P_{DEP}$	−6.81	−6.90	−0.09
(c)	**P**	**PNIR**	**PNIR−P**
Q_{CMG}	0.50	0.26	−0.24
$-P_{GACI}$	−0.26	−0.30	−0.04
$-P_{GACI}$	−0.37	−0.33	0.04
$-P_{GACW}$	−9.21	−9.84	−0.63
$-P_{GACS}$	−8.03	−8.26	−0.23
$-P_{WACS}$	−1.00	−0.93	0.07
P_{GMLT}	20.30	20.77	0.47
$-P_{GDEP}$	−1.20	−1.24	−0.04
P_{MLTG}	0.71	0.80	0.09

Thus, the decrease in averaged hydrometeors from P to PNIR was associated with the slowdown in the averaged collection of cloud water by rain and the averaged P_{IMLT}, as well as the enhancement in the averaged P_{GACW}, which may be related to the decrease in air temperature.

To demonstrate the relationship between the reduced hydrometeor decrease and falling temperature, the averaged heat budget is analyzed. Following Li et al. (1999), the horizontally averaged heat budget can be expressed by

$$\frac{\partial \overline{T}}{\partial t} = \frac{\overline{Q}_{cn}}{c_p} + \frac{\overline{Q}_R}{c_p} - \frac{\pi}{\overline{\rho}}\frac{\partial(\overline{\rho}\overline{w'\theta'})}{\partial z} - \pi\overline{w}_o\frac{\partial\overline{\theta}}{\partial z} - \overline{u}_o\frac{\partial\overline{T}_o}{\partial x} . \quad (3)$$

where T and θ are the air temperature and potential temperature, respectively; u and w are the zonal wind and vertical velocity, respectively; ρ is air density that is the function of height only; $\pi = (p/p_0)^\kappa$ with $\kappa = R/c_p$; R is the gas constant; p is pressure and p_0 = 1000 hPa; c_p is the specific heat of dry air at constant pressure; Q_{cn} is the net latent heat release through phase changes among different cloud species; Q_R is the radiative heating rate due to the convergence of net flux of solar and infrared radiative fluxes; over bar is area mean; subscript "o" denotes imposed large-scale forcing.

The strengthened averaged local atmospheric cooling from P to PNIR (Fig. 1a) was mainly associated with the

enhanced averaged longwave radiative coolingcaused by the exclusion of the radiative effects of ice clouds (Fig. 2a). The weakened averaged heat divergence corresponded to the enhanced averaged longwave radiative cooling. The release in the averaged latent heat was weakened above 7 km, whereas it was generally enhanced below 7 km.

When the radiative effects of water clouds were turned off, the averaged hydrometeors changed from an increase in PNWR to a decrease in PNCR, caused by the removal of the radiative effects of ice clouds, was associated with the averaged raindrop change from an increase in PNWR to a decrease in PNCR (Table 1). The averaged raindrop change from an increase in PNWR to a decrease in PNCR corresponded to the reduction in the averaged P_{RACW} (Table 3), which may have been caused by the decrease in air temperature. This can be demonstrated by the vertical profiles of the differences in the averaged heat budgets between PNCR and PNWR in Fig. 1b, where the enhanced averaged local atmospheric cooling occurs mainly in the upper troposphere. The intensified averaged local atmospheric cooling from PNWR to PNCR corresponded to the strengthened averaged longwave radiative cooling (Fig. 2b). The enhanced averaged local atmospheric cooling was stronger in the upper troposphere than in the mid and lower troposphere, though the averaged longwave radiative cooling was weaker in the upper troposphere than in the mid and lower troposphere. In the mid and lower troposphere, the enhanced averaged longwave radiative cooling was largely cancelled out by the increases in the release of the averaged latent heat and the convergence of vertical heat flux.

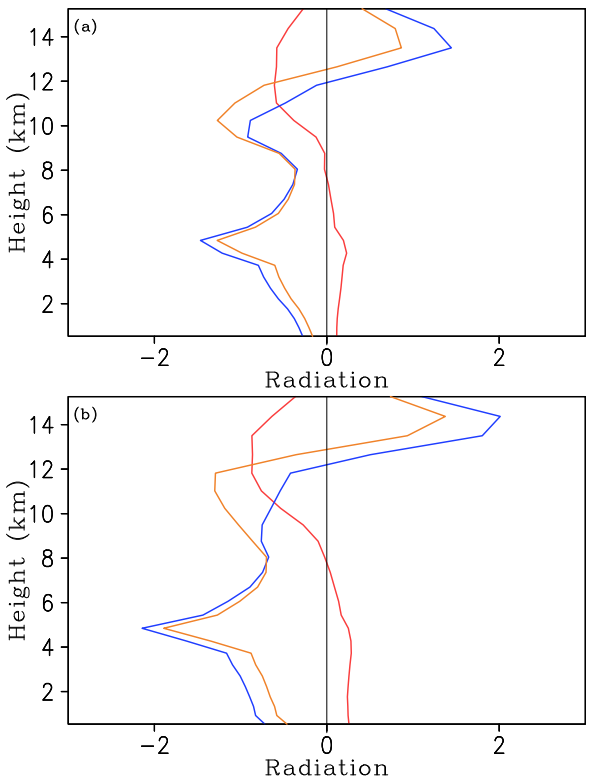

Fig. 2. Vertical profiles of the differences between (a) PNIR and P (PNIR−P) and (b) PNCR and PNWR (PNCR−PNWR) for radiation (orange) and its components of solar radiative heating (red) and infrared radiative cooling (blue), averaged over five days and the model domain. Units: °C d^{-1}.

Table 3. Breakdown of Q_{CMR} in PNWR and PNCR and their differences (PNCR−PNWR). Units: mm d^{-1}. Cloud microphysical processes listed in this table can be found in Table 1.2 in Gao and Li (2008).

	PNWR	PNCR	PNCR−PNWR
Q_{CMR}	−0.13	0.57	0.70
$-P_{\mathrm{RAUT}}$	−0.40	−0.38	0.02
$-P_{\mathrm{RACW}}$	−22.95	−22.20	0.75
$-P_{\mathrm{GACW}}(T > T_0)$	−1.40	−1.25	0.15
P_{IACR}	0.33	0.40	0.07
P_{GACR}	0.24	0.23	−0.01
P_{REVP}	12.45	12.30	−0.15
$-P_{\mathrm{SMLT}}$	−0.64	−0.62	0.02
$-P_{\mathrm{GMLT}}$	−19.43	−20.56	−1.13
P_{S}	31.73	32.58	0.85

4. Summary

The responses of pre-summer precipitation to the radiative effects of ice clouds were examined using a 2D cumulus ensemble model in this study. The cloud budgets and vertical profiles of heat budgets were analyzed to study the linkage between the precipitation rate and radiation using the model simulation data averaged over five days and the model domain. The major results can be summarized as follows:

When the radiative effects of water clouds were switched on, the removal of the radiative effects of ice clouds lowered the precipitation rate through a suppression of the hydrometeor decrease. The weakened hydrometeor decrease was associated with the decreases in the averaged P_{RACW} and the averaged P_{IMLT}, as well as the enhancement in the averaged P_{GACW}, which corresponded to the strengthened averaged local atmospheric cooling associated with the enhanced averaged longwave radiative cooling.

When the radiative effects of water clouds were turned off, the exclusion of the radiative effects of water clouds increased the precipitation rate through hydrometeor change from an increase to a decrease. The hydrometeor change was associated with the reduction in the averaged P_{RACW} caused by the strengthened averaged longwave radiative cooling in the upper troposphere.

Acknowledgements. The authors thank W.-K. TAO at NASA/GSFC for his cloud-resolving model. This work was supported by the National Key Basic Research and Development Project of China (Grant Nos. 2013CB430103 and 2015CB453201), the National Natural Science Foundation of China (Grant Nos. 41375058 and 41530427), Jiangsu Natural Science Key Project (Grant No. BK20150062), and the Priority Academic Program Development of Jiangsu Higher Education Institutions (PAPD).

REFERENCES

Chou, M.-D., and M. J. Suarez, 1994: An efficient thermal infrared radiation parameterization for use in general circulation models. NASA Tech. Memo. 104606, Vol. 3, 85 pp. [Available from NASA/Goddard Space Flight Center, Code 913, Greenbelt, MD 20771.]

Chou, M.-D., D. P. Kratz, and W. Ridgway, 1991: Infrared radiation parameterizations in numerical climate models. *J. Climate*, **4**, 424–437.

Chou, M.-D., M. J. Suarez, C.-H. Ho, M. M.-H. Yan, and K.-T. Lee, 1998: Parameterizations for cloud overlapping and shortwave single-scattering properties for use in general circulation and cloud ensemble models. *J. Climate*, **11**, 202–214.

Dudhia, J., 1989: Numerical study of convection observed during the winter monsoon experiment using a mesoscale two-dimensional model. *J. Atmos. Sci.*, **46**, 3077–3107.

Gao, S. T., and X. F. Li, 2008: *Cloud-Resolving Modeling of Convective Processes*. Springer, 206 pp.

Gao, S. T., and X. F. Li, 2010: Precipitation equations and their applications to the analysis of diurnal variation of tropical oceanic rainfall. *J. Geophys. Res.*, **115**, D08204, doi: 10.1029/2009JD012452.

Gao, S. T., F. Ping, X. F. Li, and W.-K. Tao, 2004: A convective vorticity vector associated with tropical convection: A two-dimensional cloud-resolving modeling study. *J. Geophys. Res.*, **109**, D14106, doi: 10.1029/2004JD004807.

Gao, S. T., X. P. Cui, Y. S. Zhou, and X. F. Li, 2005: Surface rainfall processes as simulated in a cloud-resolving model. *J. Geophys. Res.*, **110**, D10202, doi: 10.1029/2004JD005467.

Gao, S. T., X. P. Cui, and X. F. Li, 2009: A modeling study of diurnal rainfall variations during the 21-day period of TOGA COARE. *Adv. Atmos. Sci.*, **26**, 895–905, doi: 10.1007/s00376-009-8123-6.

Gray, W. M., and R. W. Jacobson Jr., 1977: Diurnal variation of deep cumulus convection. *Mon. Wea. Rev.*, **105**, 1171–1188.

Krueger, S. K., Q. Fu, K. N. Liou, and H.-N. S. Chin, 1995: Improvements of an ice-phase microphysics parameterization for use in numerical simulations of tropical convection. *J. Appl. Meteor.*, **34**, 281–287.

Li, X. F., and S. T. Gao, 2011: *Precipitation Modeling and Quantitative Analysis*. Springer, 240 pp.

Li, X. F., and X. Y. Shen, 2013: Rain microphysical budget in the tropical deep convective regime: A 2-D cloud-resolving modeling study. *J. Meteor. Soc. Japan*, **91**, 801–815.

Li, X. F., C.-H. Sui, K.-M. Lau, and M.-D. Chou, 1999: Large-scale forcing and cloud-radiation interaction in the tropical deep convective regime. *J. Atmos. Sci.*, **56**, 3028–3042.

Li, X. F., C.-H. Sui, and K.-M. Lau, 2002: Dominant cloud microphysical processes in a tropical oceanic convective system: A 2D cloud resolving modeling study. *Mon. Wea. Rev.*, **130**, 2481–2491.

Li, X. F., X. Y. Shen, and J. Liu, 2011: A partitioning analysis of tropical rainfall based on cloud budget. *Atmos. Res.*, **102**, 444–451.

Li, X. F., G. Q. Zhai, S. T. Gao, and X. Y. Shen, 2014: A new convective-stratiform precipitation rate separation scheme. *Atmos. Sci. Lett.*, **15**, 245–251.

Li, X. F., P. J. Zhu, G. Q. Zhai, R. Liu, X. Y. Shen, W. Huang, and D. H. Wang, 2016: Testing parameterization schemes for simulating depositional growth of ice crystal using Koenig and Takahashi parameters: A pre-summer rainfall case study over southern China. *Atmos. Sci. Lett.*, **17**, 3–12, doi: 10.1002/asl.591.

Lilly, D. K., 1988: Cirrus outflow dynamics. *J. Atmos. Sci.*, **45**, 1594–1605.

Lin, Y.-L., R. D. Farley, and H. D. Orville, 1983: Bulk parameterization of the snow field in a cloud model. *J. Climate Appl. Meteor.*, **22**, 1065–1092.

Liu, J., X. Y. Shen, and X. F. Li, 2014: Radiative effects of water clouds on heat, cloud microphysical and surface rainfall budgets associated with pre-summer torrential rainfall. *Terrestrial, Atmospheric and Oceanic Sciences*, **25**, 39–48.

Rutledge, S. A., and P. V. Hobbs, 1983: The mesoscale and microscale structure and organization of clouds and precipitation in midlatitude cyclones. Part VIII: A model for the "seeder-feeder" process in warm-frontal rainbands. *J. Atmos. Sci.*, **40**, 1185–1206.

Rutledge, S. A., and P. V. Hobbs, 1984: The mesoscale and microscale structure and organization of clouds and precipitation in midlatitude cyclones. Part XII: A diagnostic modeling study of precipitation development in narrow cold-frontal rainbands. *J. Atmos. Sci.*, **41**, 2949–2972.

Shen, X. Y., Y. Wang, N. Zhang, and X. F. Li, 2010: Precipitation and cloud statistics in the deep tropical convective regime. *J. Geophys. Res.*, **115**, D24205, doi: 10.1029/2010JD014481.

Shen, X. Y., Y. Wang, and X. F. Li, 2011a: Radiative effects of water clouds on rainfall responses to the large-scale forcing during pre-summer heavy rainfall over southern China. *Atmos. Res.*, **99**, 120–128.

Shen, X. Y., Y. Wang, and X. F. Li, 2011b: Effects of vertical wind shear and cloud radiative processes on responses of rainfall to the large-scale forcing during pre-summer heavy rainfall over southern China. *Quart. J. Roy. Meteor. Soc.*, **137**, 236–249.

Shen, X. Y., N. Zhang, and X. F. Li, 2011c: Effects of large-scale forcing and ice clouds on pre-summer heavy rainfall over southern China in June 2008: A partitioning analysis based on surface rainfall budget. *Atmos. Res.*, **101**, 155–163.

Shen, X. Y., J. Liu, and X. F. Li, 2012: Torrential rainfall responses to ice microphysical processes during pre-summer heavy rainfall over southern China. *Adv. Atmos. Sci.*, **29**, 493–500, doi: 10.1007/s00376-011-1122-4.

Shen, X. Y., W. Huang, T. Qing, W. Y. Huang, and X. F. Li, 2014: A modified scheme that parameterizes depositional growth of ice crystal: A modeling study of pre-summer torrential rainfall case over southern China. *Atmos. Res.*, **138**, 293–300.

Soong, S. T., and Y. Ogura, 1980: Response of tradewind cumuli to large-scale processes. *J. Atmos. Sci.*, **37**, 2035–2050.

Soong, S. T., and W.-K. Tao, 1980: Response of deep tropical cumulus clouds to mesoscale processes. *J. Atmos. Sci.*, **37**, 2016–2034.

Sui, C.-H., K.-M. Lau, W.-K. Tao, and J. Simpson, 1994: The tropical water and energy cycles in a cumulus ensemble model. Part I: Equilibrium climate. *J. Atmos. Sci.*, **51**, 711–728.

Sui, C.-H., K.-M. Lau, Y. N. Takayabu, and D. A. Short, 1997: Diurnal variations in tropical oceanic cumulus convection during TOGA COARE. *J. Atmos. Sci.*, **54**, 639–655.

Sui, C.-H., X. Li, and K.-M. Lau, 1998: Radiative-convective processes in simulated diurnal variations of tropical oceanic convection. *J. Atmos. Sci.*, **55**, 2345–2359.

Tao, W.-K., and J. Simpson, 1993: Goddard Cumulus Ensemble model. Part I: Model description. *Terrestrial, Atmospheric & Oceanic Sciences*, **4**, 35–72.

Tao, W.-K, J. Simpson, and M. McCumber, 1989: An ice-water

saturation adjustment. *Mon. Wea. Rev.*, **117**, 231–235.

Tao, W.-K., J. Simpson, C.-H. Sui, B. Ferrier, S. Lang, J. Scala, M.-D. Chou, and K. Pickering, 1993: Heating, moisture, and water budgets of tropical and midlatitude squall lines: Comparisons and sensitivity to longwave radiation. *J. Atmos. Sci.*, **50**, 673–690.

Wang, D. H., X. F. Li, W.-K. Tao, Y. Liu, and H. G. Zhou, 2009a: Torrential rainfall processes associated with a landfall of severe tropical storm Bilis (2006): A two-dimensional cloud-resolving modeling study. *Atmos. Res.*, **91**, 94–104.

Wang, D. H., X. F. Li, W.-K. Tao, and Y. Wang, 2009b: Effects of vertical wind shear on convective development during a landfall of severe tropical storm Bilis (2006). *Atmos. Res.*, **94**, 270–275.

Wang, D. H., X. F. Li, and W.-K. Tao, 2010a: Responses of vertical structures in convective and stratiform regions to large-scale forcing during the landfall of severe tropical storm Bilis (2006). *Adv. Atmos. Sci.*, **27**, 33–46, doi: 10.1007/s00376-009-8139-y.

Wang, Y., X. Y. Shen, and X. F. Li, 2010b: Microphysical and radiative effects of ice clouds on responses of rainfall to the large-scale forcing during pre-summer heavy rainfall over southern China. *Atmos. Res.*, **97**, 35–46.